https://doi.org/10.5194/essd-2020-63
Preprint. Discussion started: 17 June 2020

Open Access Earth System Science Data Discussions

A Long Term (2005 - 2019) Eddy Covariance Data Set of CO_2 and H_2O Fluxes from the Tibetan Alpine Steppe

Felix Nieberding[1,2], Christian Wille[2], Gerardo Fratini[3], Magnus O. Asmussen[1], Yuyang Wang[4,5,6], Yaoming Ma[4,5,6], and Torsten Sachs[2,1]

[1]Technische Universität Braunschweig, Germany
[2]GFZ German Research Centre for Geosciences, Potsdam, Germany
[3]LI-COR Biosciences Inc., Lincoln, Nebraska, USA
[4]Key Laboratory of Tibetan Environment Changes and Land Surface Processes, Institute of Tibetan Plateau Research, Chinese Academy of Sciences, Beijing, China
[5]CAS Center for Excellence in Tibetan Plateau Earth Sciences, Beijing, China
[6]University of Chinese Academy of Sciences, Beijing, China

Correspondence: Felix Nieberding (f.nieberding@tu-braunschweig.de), Yaoming Ma (ymma@itpcas.ac.cn)

Abstract. The Tibetan alpine steppe ecosystem covers an area of roughly 800,000 km^2, containing up to 3.3 % soil organic carbon in the uppermost 30 cm, summing up to 1.93 Pg C for the Tibet Autonomous Region only (472,037 km^2). With temperatures rising two to three times faster than the global average, these carbon stocks are at risk of loss due to enhanced soil respiration. The remote location and the harsh environmental conditions on the Tibetan Plateau (TP) make it challenging to derive accurate data on ecosystem-atmosphere exchange of carbon dioxide (CO_2) and water vapor (H_2O). Here, we provide the first multi-year data set of CO_2 and H_2O fluxes from the central Tibetan alpine steppe ecosystem, measured in situ using the eddy covariance technique. The calculated fluxes were rigorously quality checked and carefully corrected for a drift in concentration measurements and gas analyzer self heating during cold conditions. A wind field analysis was conducted to identify influences of adjacent buildings on the turbulence regime and to exclude the disturbed fluxes from subsequent computations. The presented CO_2 fluxes were additionally gap filled using a standardized approach. The very low net carbon uptake across the 15-year data set highlights the special vulnerability of the Tibetan alpine steppe ecosystem to become a source of CO_2 due to global warming. The data is freely available (https://www.doi.org/10.5281/zenodo.3733203, Nieberding et al., 2020b) and may help to better understand the role of the Tibetan alpine steppe in the global carbon-climate feedback.

https://doi.org/10.5194/essd-2020-63
Preprint. Discussion started: 17 June 2020

1 Introduction

The Tibetan Plateau is also called "The Third Pole" because it harbors the third largest ice mass on earth, right after the polar regions (Qiu, 2008). It has an area of about 2.5 million km^2 at an average elevation of > 4000 m above sea level and includes the entire southwestern Chinese provinces of Tibet and Qinghai, parts of Gansu, Yunnan, Sichuan and neighboring countries. Similarly to the northern high latitudes, the TP is warming considerably faster than the global average, with air temperatures rising at a rate of 0.35 K per decade (from 1970 to 2014) (Yao et al., 2019). At the same time, the TP is experiencing changes in precipitation rates, which alter its water cycle, possibly affecting 1.65 billion people across South East Asia (Cuo and Zhang, 2017). While precipitation is reduced on the southern and eastern margins of the TP, it is enhanced in the central area, partly due to higher temperatures and thus enhanced evaporation, leading to more effective water recycling (Yang et al., 2014; Wang et al., 2018). The majority of the TP is covered by the biggest pastoralist system in the world, the so called steppe-meadow ecotone, consisting of 450,000 km^2 *Kobresia* (syn. *Carex*) *pygmaea* pastures and 800,000 km^2 alpine steppe ecosystem (Miehe et al., 2011, 2019). With decreasing precipitation to the west, the *K. pygmaea* pastures are replaced by alpine steppe ecosystems. With 14-48 % mean total vegetation cover, the alpine steppe exhibits considerably less above-ground biomass than the *K. pygmaea* pastures. At least in the eastern part, the alpine steppe soils still contain an almost 30 cm thick, organically rich layer, which consists of up to 3.3 % soil organic carbon (SOC), summing up to 1.93 Pg C for the Tibet Autonomous Region only (472,037 km^2) (Zhou et al., 2019). Hence, the response of CO_2 and H_2O fluxes to environmental changes in the Tibetan Plateau grasslands are crucial for the water cycling in greater Asia and the global carbon budget, respectively. While the carbon cycling in *Kobresia* pastures has been studied extensively, the alpine steppe ecosystem remains underrepresented, particularly with regard to long term observations.

This study presents nearly 15 years of eddy covariance data from an alpine steppe ecosystem on the central Tibetan Plateau. The aim of this study is to calculate consistent CO_2 fluxes while following standardized quality control methods to allow for comparability between the different years of our record and with other data sets. To ensure meaningful estimates of ecosystem-atmosphere exchange, careful application of the following correction procedures and analyses was necessary: (1) Due to the remote location, continuous maintenance of the EC system was not always possible, so that cleaning and calibration of the sensors was performed irregularly. Furthermore, the high proportion of bare soil and high wind speeds led to accumulation of dirt in the measurement path of the IRGA. The installation of the sensor in such a challenging environment resulted in a considerable drift in CO_2 and H_2O gas density measurements. If not accounted for, this concentration bias may distort the estimation of the carbon uptake. We applied a modified drift correction procedure following Fratini et al. (2014) which, instead of a linear interpolation between calibration dates, uses the CO_2 concentration measurements from the Mauna Loa atmospheric observatory as reference time series. (2) We applied rigorous low frequency quality filtering to retain only flux measurements which represent actual physical processes. (3) During the long measurement period, there were several buildings constructed in the near vicinity of the EC system. We investigated the influence of these obstacles on the turbulent flow regime and conducted a footprint analysis to identify fluxes with uncertain land cover contribution and exclude them from subsequent computations. (4) We applied a correction for instrument surface heating during cold conditions (hereafter called sensor self heating correction

https://doi.org/10.5194/essd-2020-63
Preprint. Discussion started: 17 June 2020

Open Access Earth System Science Data Discussions

after Burba et al. (2008)), following the approach of Oechel et al. (2014). (5) Subsequently, we applied the traditional and widely used gap filling procedure following Reichstein et al. (2005) to provide a more complete overview of the annual net ecosystem CO_2 exchange. (6) We estimated the random uncertainty following Finkelstein and Sims (2001) and analyzed the error propagation through the WPL correction to get an estimation of the accuracy of the measurements.

2 Material and methods

2.1 Site description and measurements

The Nam Co Station for Multi-sphere Observation and Research (NAMORS, Chinese Academy of Sciences) is located at 4730 m a.s.l., about 220 km north of the Tibetan capital Lhasa (30° 46' N, 90° 57' S; Fig. 1). It is situated on an almost flat plain between the ENE-WSW oriented Nyainqêntanglha range in 15 km distance to the SSE and lake Nam Co about 1 km to the NW. The climate at Nam Co is characterized by strong seasonality, with long, cold winters and short but moist summers. The mean annual air temperature measured at the NAMORS research station between 2005 and 2019 was -0.2 °C. During winter, the Westerlies control the general circulation and lead to cold and dry weather, with temperature minima below -20 °C. Although snow storms do occur during winter time, a closed snow cover is seldom reached for longer time periods. In springtime, the TP heats up and allows the melt water to percolate to deeper soil layers. The drought situation increases gradually until the monsoon rains arrive, typically between May and June. The southern branch of the westerlies needs to shift northward of the Tibetan Plateau so that the humid air masses from the intertropical convergence zone can reach the plateau along meridional river gorges, thus increasing precipitation notably. The annual precipitation ranges from 291 to 568 mm (mean = 403 mm), with the majority occurring during the monsoon season from May to October. During autumn, weather shifts again to clear, cold and dry conditions (Yao et al., 2013). The study site is covered by degraded *Stipa purpurea* alpine steppe vegetation, which includes species from the families *Artemisia*, *Stipa*, *Poa*, *Festuca* and *Carex* (Li et al., 2018; Miehe et al., 2011). The vegetation heights do not exceed 5 cm due to heavy grazing by yak and sheep and the plant cover is usually less than 50 % (Nölling, 2006). The substrate is mostly soil and loess. The (micro-) meteorological measurements at the NAMORS site were established in 2005 by the Institute of Tibetan Plateau Research (ITP), Chinese Academy of Sciences (CAS) (Ma et al., 2009). The measurement complex is comprised of a 52 m tall Planetary Boundary Layer (PBL) tower measuring air temperature and relative humidity in 5 different heights and wind speed and wind direction in 3 different heights (1.5 m, 2 m, 4 m, 10 m, 20 m and 1.5 m, 10 m, 20 m, respectively). The 3 m Eddy Covariance measurement tower is equipped with a CSat3 ultrasonic anomometer (USA) and a Li-7500 open path infrared gas analyzer (IRGA). The separation between the two sensors is 23 cm. The site is further supplemented with measurements of soil moisture and soil temperature (0 cm, -10 cm, -20 cm, -40 cm, -80 cm, -160 cm), soil heat flux (-10 cm, -20 cm) and radiation (short and long wave downward and upward radiation, global radiation), precipitation and air pressure measurements. In 2013 the station was extended for a photosynthetic photon flux density sensor (PPFD) (Zhu et al., 2015). For detailed information about available measurements and sensor types please see Ma et al. (2009).

https://doi.org/10.5194/essd-2020-63
Preprint. Discussion started: 17 June 2020

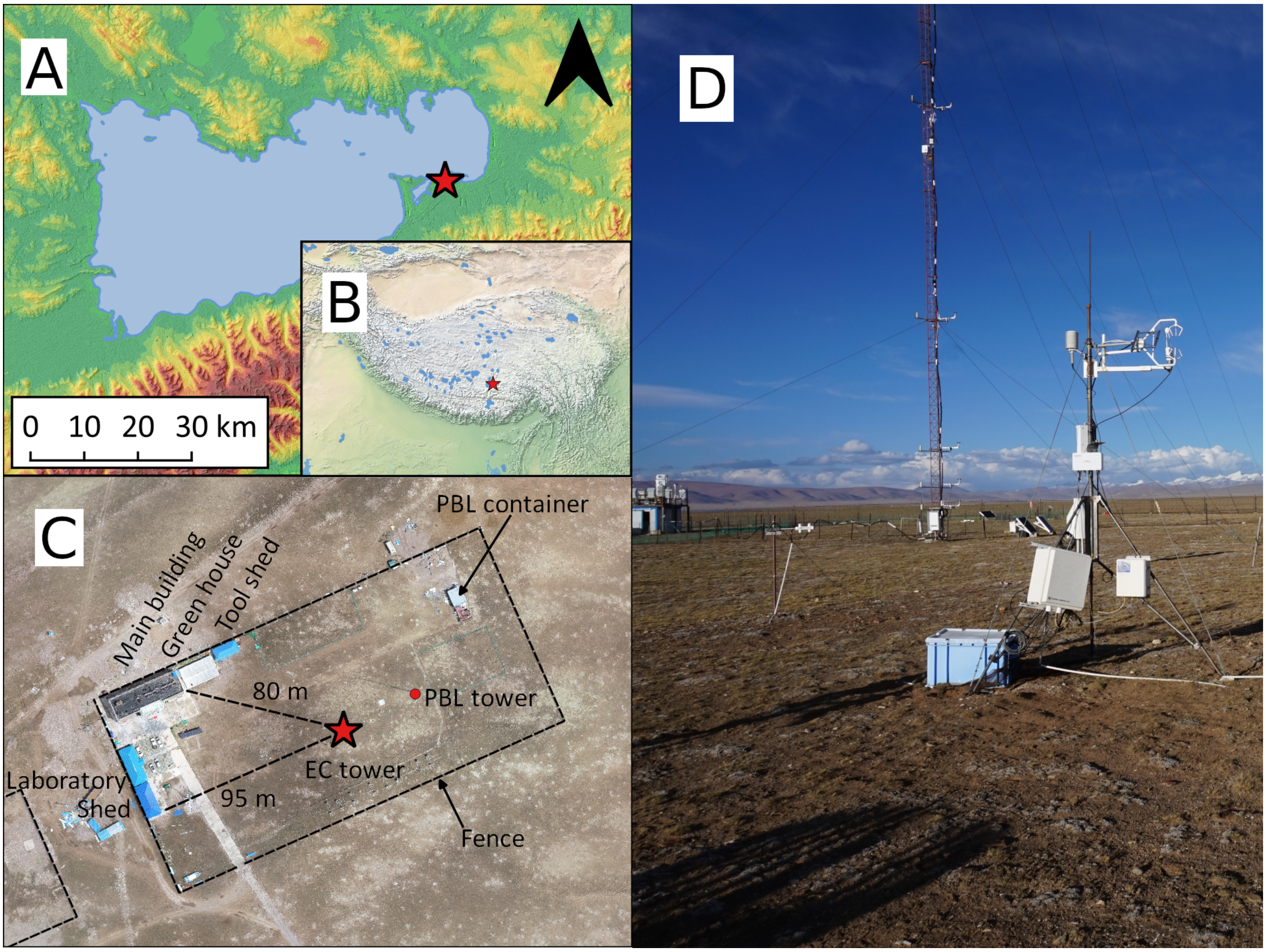

Figure 1. (A) Study site at the NAMORS station close to lake Nam Co (ASTER GDEM V3, NASA/METI/AIST/Japan Spacesystems, and U.S./Japan ASTER Science Team, 2019). (B) Overview map showing the location on the Tibetan Plateau, made with Natural Earth. (C) Aerial image of the NAMORS station with the main features in July 2019. Images by Guoshuai Zhang. (D) Photo of the EC system (front), PBL tower and part of the PBL container (back) in May 2019. Photo by Felix Nieberding.

2.2 EC raw data processing

The Eddy Covariance method is a direct micrometeorological approach to estimate turbulent exchange of heat, momentum and matter between the atmosphere and the underlying surface (Aubinet et al., 2012). It is a common approach to estimate the net ecosystem CO_2 exchange (NEE), which is the sum of carbon uptake via photosynthesis of green vegetation (Gross Primary Production, hereafter GPP) and carbon release through autotrophic and heterotrophic respiration (Ecosystem Respiration, hereafter R_{eco}). The turbulence measurements were conducted with a Csat3 ultrasonic anemometer measuring the three-dimensional wind vector. A Li-7500 infrared gas analyzer was placed in close vicinity to the anemometer, measuring

https://doi.org/10.5194/essd-2020-63
Preprint. Discussion started: 17 June 2020

Table 1. Flux data processing procedure using EddyPro software (v. 7.0.4, LI-COR Inc.)

Despiking following Vickers and Mahrt (1997) with the following plausibility ranges: W = 5.0 σ, CO_2 = 3.5 σ, H_2O = 3.5 σ, sonic temperature = 3.5 σ
Amplitude resolution: Range of variation = 3.5 σ, number of bins = 100, accepted empty bins = 70 %
Drop-outs: extreme bins = 10 percentile, accepted central drop-outs = 10 %, accepted extreme drop-outs = 6 %
Discontinuities with the following hard flags (hf) and soft flags (sf): U: hf = 4.0, sf = 2.7; W: hf = 2.0, sf = 1.3; Ts: hf = 4.0, sf = 2.7; CO_2: hf = 40.0, sf = 27.0; H_2O: hf = 40.0, sf = 30.0; variances: hf = 3.0, sf = 2.0
Skewness and **kurtosis** with the following hf and sf: Skw limits: hf = $\pm$ 2.0, sf = $\pm$ 1.0; kur lower limits: hf = 1.0, sf = 2.0; kur upper limits: hf = 8.0, sf = 5.0
Steadiness of horizontal wind: Accepted wind relative instationarity = 0.5
Axis rotation: Planar fit using 3 wind sectors (0° - 80°, 80° - 230 °, 230° - 360 °)
Detrending method: Block averaging
Time lags optimization: Covariance maximization with default $\pm$ 1 s
Correction for **air density fluctuations**: Application of WPL terms to fluxes (Webb et al., 1980)
Spectral corrections: Analytic high-pass filtering (Moncrieff et al., 2005) and analytic low-pass filtering (Moncrieff et al., 1997)

the CO_2 concentration of the up- and downward moving air parcels. The acquisition frequency is 10 Hz and the fluxes were calculated for every 30-min interval using the raw data processing software EddyPro (v7.0.6, LI-COR Inc.). Table 1 shows the processing and correction procedure which follows standardized and well tested methods including despiking, axis rotation, detrending and data quality flagging based on stationarity, instrument performance, as well as integral turbulence characteristics (Foken and Wichura, 1996; Foken et al., 2004). The data flagging policy is following Mauder and Foken (2006), with "0" for high quality fluxes, "1" for intermediate quality fluxes and "2" for poor quality fluxes. Following the usual atmospheric convention, positive values represent fluxes moving away from the surface and negative values represent fluxes moving towards the surface.

2.3 Drift correction

The Li-7500 is a so called "dual wavelength, single path" instrument that estimates CO_2 and water vapor density (ρ_c and ρ_v, respectively) from the amount of radiation passing an ambient air volume in a gas absorbing wavelength, relative to the amount of radiation passing the same sample volume in a non-absorbing reference wavelength. The absorbing wavelengths are 4.25 µm and 2.59 µm for CO_2 and H_2O, respectively, with both sharing the same non-absorbing reference wavelength of

https://doi.org/10.5194/essd-2020-63
Preprint. Discussion started: 17 June 2020

3.95 µm (Serrano-Ortiz et al., 2008). Absorptance is then converted into an estimate of gas number density by means of an instrument specific curvilinear calibration curve. Due to small sensor specific variations in sources, lens chromatic aberrations, variations in optical filters, detector heterogeneities, and other things, the relationship between absorptance and density is not theoretically predictable but has to be empirically determined for every individual sensor. Following Fratini et al. (2014), every instrument has its own factory derived calibration function (F) to describe the exact relationship between absorptance (a) and density (ρ), depending on air pressure (Pa):

$$\rho = PF(\frac{a}{Pa}) \tag{1}$$

Lens contamination due to mineral dust in the optical path more strongly affects smaller wavelengths, leading to an underestimation of ρ_c and an overestimation of ρ_v. These drift errors are usually not accounted for under the assumption, that a slow drift in mean gas concentrations (i.e. over several weeks to months) does not affect the estimation of turbulent fluctuations and, hence, of covariances. This is however not the case. In fact, Serrano-Ortiz et al. (2008) estimated, that a drift in concentration measurements will propagate into an overestimation of the carbon dioxide uptake via the WPL correction. They also showed, that this error is not evenly distributed but has a greater affect during daytime and summer, when sensible heat fluxes are large. Fratini et al. (2014) have shown, that errors in mean concentrations leak into errors in fluxes on account of amplified or dampened estimated fluctuations. Fratini et al. (2014) have also shown that both these effects can be eliminated, possibly completely, when the drift in gas concentration is corrected before raw data processing. Therefore, the offset between measured and reference (i.e. "real") gas concentrations has to be quantified and converted into the corresponding zero offset absorptance biases. Fratini et al. (2014) estimated the reference gas concentrations through linear interpolation of the zero absorptance offset between individual calibration dates, thereby assuming a constant increase of the bias. Due to the remote location on the Tibetan Plateau, user calibrations of the sensor were not performed with due regularity, making this approach not feasible in our case. Instead, we used the daily mean CO_2 mixing ratios from the Mauna Loa atmospheric observatory (years 2005-2018, NOAA ESRL Global Monitoring Division) to fit a sine-cosine model, which was then used to determine the offset of our measurements. We used the differences between the daily median measured CO_2 concentrations and the model, which was then repeated 48 times, yielding a single value for every 30-min interval. Using a sine-cosine model preserves the naturally occurring annual fluctuations in CO_2 concentrations better than, e.g. a linear model would do. The offset in H_2O mixing ratios was determined using auxiliary low frequency measurements of relative humidity, temperature and air pressure. We can use Eq. (2) (which is Eq. (10) from Fratini et al., 2014) to calculate the true absorptance (a) from measured absorptance (a_m) and any absorptance offset (a_0), which is then converted back to densities or mixing ratios.

$$a = \frac{a_m - a_0}{1 - a_0} \tag{2}$$

The time series of absorptance offset values were imported as dynamic metadata file in EddyPro. It is used together with the sensor specific calibration information to repeat raw data calculation of the fluxes and subsequent corrections, including application of WPL terms following the methodology in Sect. 2.2. Note that all conversions between absorptance and number density require the calibration function of the specific instrument.

https://doi.org/10.5194/essd-2020-63
Preprint. Discussion started: 17 June 2020

2.4 Quality filtering

The correct application of the eddy covariance method requires a wide range of assumptions and works only within certain conditions. To ensure meaningful flux calculations, the raw data needs to be tested and flagged very thoroughly. We used the quality flags and tests implemented in EddyPro and applied additional filtering for low frequency outliers using openeddy R package from Ladislav Šigut, who implemented the quality control procedure following Mauder et al. (2013). The flagging scheme remains the same as above with "0" for high quality fluxes, "1" for intermediate quality fluxes and "2" for poor quality fluxes. As a first step, we manually removed periods with obvious sensor malfunctioning, especially in 2012 and 2018. CO_2 and H_2O fluxes and their respective densities were additionally checked for repeating values as they are a sign of malfunctioning equipment. We furthermore extracted hard flags of skewness and kurtosis and of discontinuities (see Table 1) and combined all flags to a preliminary composite which was used as a prerequisite for subsequent low frequency despiking of the flux time series. To account for seasonal variations, despiking is done within blocks of 13 consecutive days by comparing each record (v_i) with its neighbors via double differencing to produce its score x:

$$x = (v_i - v_{i-1}) - (v_{i+1} - v_i) \tag{3}$$

A measurement gets flagged if x is larger or smaller than the median of the scores (M_x) $\pm$ the scaled absolute median *MAD*:

$$M_x + \frac{z * MAD}{0.6745} < x < M_x - \frac{z * MAD}{0.6745} \tag{4}$$

with MAD being defined as:

$$MAD = median(x - M_x) \tag{5}$$

The constant 0.6745 in Eq. (4) corresponds to the Gaussian distribution and allows for comparability of MAD with the scaling factor z, which determines how rigorous the algorithm screens for outliers (Papale et al., 2006). The lower the value, the stricter the screening, with our setting left to the default $z = 7$. This procedure was repeated iteratively 10 times or until no outliers were detected anymore. For every measurement, the flags were combined to an overall quality flag and fluxes and concentrations with poor quality (flag = "2") were removed from subsequent computations.

2.5 Wind field analysis

In order to conduct meaningful estimations of the fluxes, the area "seen" by the measurement should represent the ecosystem of interest and the flow regime should be as undisturbed as possible (Aubinet et al., 2012). During the long measuring period, spanning nearly 15 years, several buildings and scientific infrastructure were constructed in close vicinity of the eddy covariance tower. During the development of the NAMORS, from the foundation with only a few tents in 2005 to a well-equipped research station in 2019, we approximated five times with significant changes in constructions (2). In 2009 the PBL container, the shed and the solar panel were set up. In 2010 the main building and the green house were constructed. In 2012 the shed was rotated to become the laboratory and the tool shed next to the greenhouse was added. Finally, in 2019 the garage was

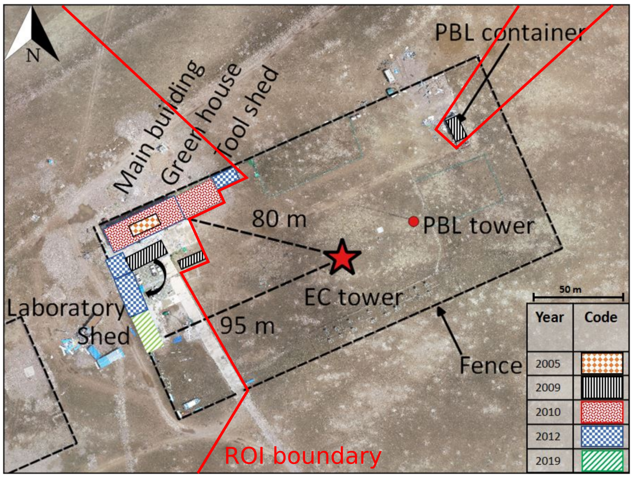

Figure 2. Map of the NAMORS station showing the identified changes in construction from 2005 to 2019 and the ROI boundaries. Aerial images provided by Guoshuai Zhang.

relocated and extended south of the laboratory and the solar panels were removed. To account for possibly disturbed turbulence, we applied the planar fit axis rotation for three different wind sectors during flux calculation (see Sect. 2.2). To assess possible influences on the flow and turbulence regime, we analyzed the wind direction distribution of the mean wind speed and the turbulent kinetic energy. Furthermore, we estimated the source area of the flux measurements by calculating cumulative footprints using the model of Kormann and Meixner (2001). This footprint model was developed for non-neutral atmospheric conditions, therefore all measurements were checked for the stability parameter $(z-d)/L \neq 0$. The model relates a flux to a certain direction in a certain distance around the EC station, depending on the measurement height, wind direction and wind speed, friction velocity, atmospheric stability and the cross stream wind component. The cummulative footprints (Fig. 5) were calculated and plotted using FREddyPro R package. However, EddyPro also allows for the computation of flux footprints using Kormann and Meixner (2001) but supplies only the distances of flux contributions (10 %, 30 %, 50 %, 70 %, 90 %) in wind direction. By defining a region of interest (ROI) we excluded fluxes if the contribution from disturbed areas (red squares in Fig. 5) was ≥ 50 % from further analyses.

2.6 Sensor self heating correction

When using an open path IRGA, it is necessary to correct for air density fluctuations caused by fluctuations of temperature and water vapor in the measurement path. The WPL correction compensates for the naturally occurring density fluctuations and should be applied in any case (Webb et al., 1980). Furthermore, especially during cold conditions (low temperatures below -10 °C), an apparent CO_2 uptake may be measured, which is caused by conductive, convective, and radiative heat exchange processes happening in the measurement path (Burba et al., 2008). These stem from heating of internal electronics during normal operation, as well as solar radiation encountered by different instrument parts surrounding the open sampling path

https://doi.org/10.5194/essd-2020-63
Preprint. Discussion started: 17 June 2020

Open Access Earth System Science Data Discussions

of the sensor. This correction is necessary for pre-2010 models of the Li-7500 or for newer instruments (e.g. Li-7500A, Li-7500RS) with summer setting but used in a very cold environment (Oechel et al., 2014). Although the size of the heating correction is quite small (i.e. 10-50 times smaller than the WPL-correction) the small bias can lead to an overestimation of net ecosystem CO_2 uptake when integrating over long periods in cold environments (Oechel et al., 2014). Burba et al. (2008) developed a correction procedure which is well tested and fully implemented in the EddyPro software. The procedure depends on a range of correction factors, which were developed from the original sensor setup in Nebraska, USA. Our study site on the Tibetan Plateau displays different environmental conditions than those in which the correction was tested, namely an inclined IRGA, lower ambient temperatures and strong winds, as well as possible snow and ice deposits on parts of the instrument. No independent gas concentration measurements are available from our study site which could be used for fine tuning of the air density correction. Hence, we applied the approach by Oechel et al. (2014), who developed an empirical method to calibrate the correction of EC measurements, originally for a sensor in Alaska. We made the same assumptions as Oechel et al. (2014) concerning the relationship between the vertically aligned sensor Burba et al. (2008) used in the original method in Nebraska in comparison to our aligned sensor in Tibet: The sensor consists of a bottom, cylinder-shaped part and a top, ball-shaped part which are differently exposed to ambient conditions (e.g. solar radiation) depending on the inclination of the sensor. While the top, ball-shaped part of the sensor is about equally exposed in Nebraska and Tibet, we assume the inclined bottom cylinder in Tibet to be more exposed to radiation than the vertical aligned bottom cylinder in Nebraska. Its temperature (T_{botTI}) is a combination of the bottom cylinder temperature in Nebraska (T_{botNE}) and the top ball temperature in Nebraska (T_{topNE}) adjusted with a weighting factor x.

$$T_{botTI} = xT_{botNE} + (1-x)T_{topNE} \tag{6}$$

The weighting factor x has to be parameterized by calculating the sensor self heating correction using Method 4 (submethod: linear regression with air temperature Burba et al., 2008) for multiple weighting factors. The optimal weighting factor is selected on the basis of two criteria: First, periods have to be identified when a change in CO_2 efflux with temperature can be assumed to be negligible. For our study site on the Tibetan Plateau, we assume negligible CO_2 efflux when air temperature is below -15 °C and soil moisture below 2 % during the months of January and February. The ground can be regarded as continuously frozen since two months, with mean air temperatures below 0 °C at least since November. By then, freezing should have pushed any excess CO_2 out of the soil. During these cold conditions, the flux-to-air temperature slope was calculated for every weighting factor (0-100). The CO_2 fluxes should not change with temperature during these cold conditions, hence the closer the slope to zero, the better. Second, the direction of the corrections for every weighting factor was examined for periods where a negative correction would be implausible. Because the electronics of the pre-2010 model of the Li-7500 are kept at about +30 °C, the sensor should on average be warmer than the ambient air. A negative daily correction would implicate, that the ambient air is warmer than the sensor surface which is implausible at temperatures below 0 °C. Hence, the number of negative daily corrections at air temperatures below 0 °C should be small, which is the second criterion to find the optimal weighting factor. The optimal weighting factor is then used to correct all measurements when ambient temperature is below

https://doi.org/10.5194/essd-2020-63
Preprint. Discussion started: 17 June 2020

0 °C. We used a radiation threshold of 5 W m^{-2} to distinguish between daytime and nighttime. The method is described in detail in Oechel et al. (2014) and the R script with the exact calculations can be found in the supplementary material.

2.7 Gap filling

In order to obtain a CO_2 flux time series as complete as possible, we filled the data gaps using the marginal distribution sampling (MDS) algorithm (Falge et al., 2001; Reichstein et al., 2005), implemented in the REddyProc R package by Wutzler et al. (2018). Depending on the length of the data gap and the availability of the meteorological input variables radiation (Rg), air temperature (Tair) and water vapor deficit (VPD), the missing CO_2 flux values are derived from a look up table (LUT) or from mean diurnal course (MDC). The LUT approach replaces the missing value with the average value under similar meteorological conditions within a certain time window. Meteorological conditions are similar if Rg deviates not further than 50 W m^{-2}, Tair not further than 2.5 °C and VPD not further than 5.0 hPa. If no similar conditions can be found within an appropriate time window, the missing value is replaced using the average value at the same time of the day (1 hour) (MDC). If the missing value can not be filled during the initial time period (7 - 14 days), the time window size is increased and the procedure repeated until the value can be filled or the data gap gets too long for reliable gap filling (i.e. > 60 days). As horizontal wind speeds are generally very high (lowest percentile = 0.47 m s^{-1}) at our study site, we did not filter for low friction velocity. The full MDS algorithm is described in Wutzler et al. (2018) and the R script used in this study can be found in the appendix.

To estimate the uncertainty of the gap-filling procedure, we used the method implemented in REddyProc R package, which, besides filling real gaps, creates artificial gaps from otherwise available data and fills them in the same way as if it was a real gap (see section 2.7). The model-value residual should be considered when aggregating the gap-filled time series to daily or annual estimates of NEE, GPP and R_{eco}. We included the filled values for the artificially created data gaps, as well as quality flags for the gap filling procedure, with "0" for measured data, "1" for high reliability, "2" for intermediate reliability and "3" for poor reliability of the gap-filled values.

2.8 Flux uncertainty estimation

As with all measurements, the reported fluxes are subject to uncertainty, consisting of a systematic and a random part. Systematic uncertainties may occur e.g. from having an imperfect measurement setup or, like in our case, due to limited maintenance and calibration of the sensors (see section 2.3). We applied a wide range of methods to filter and compensate for systematic errors. Most importantly, we tested for fulfillment of basic EC assumptions using integral turbulence characteristics and steady state test (e.g., Foken and Wichura, 1996) and compensated for air density fluctuations and high- and low-frequency losses (see Sect. 2.2, 2.4 and 2.6). In contrast to systematic uncertainties, random errors do not bias the flux in any direction but reduce the overall confidence (i.e. precision) of the reported values (Richardson et al., 2012). Random uncertainties mainly arise from the stochastic nature of turbulence, footprint variability, as well as from instrument noise and the resolution at which samples are recorded (Richardson et al., 2012). Hence, it is important to estimate the random uncertainty, especially in places with rather low magnitude of fluxes, as it is in our case. We estimated the random flux error using the mathematically rigorous and fully implemented approach by Finkelstein and Sims (2001). This method calculates the random flux errors arising from

https://doi.org/10.5194/essd-2020-63
Preprint. Discussion started: 17 June 2020

insufficient sampling of large eddies with high spectral energy, the so-called sampling error. As these large turbulences appear irregularly during sampling, the error is random and can be estimated. First, the so-called Integral Turbulence time-Scale (ITS) is calculated. Basically, the ITS is the covariance between vertical wind velocity and gas concentration as a function of lag time between these two time series (Holl et al., 2019). With increasing time lag, the cross correlation function typically decreases towards values close to zero, indicating an increasing non-correlation of the two time series. In practice, the correlation function must be stopped, otherwise it would go infinitely towards zero. We stopped the integral as soon as the cross-correlation function (which always starts at 1) crosses the x-axis (i.e. first crossing 0). In case the cross-correlation function would never cross the x axis, a default time value can be provided at which the function is stopped. We set this "maximum correlation period" to 5 s in order to keep computational performance high. Once the ITS is calculated, the random uncertainty of the fluxes can be estimated based on the calculation of the "variance of covariance" (Finkelstein and Sims, 2001).

It is important to note, that the random error estimate applies to the uncorrected fluxes, i.e. before correction for spectral attenuation and air density fluctuations. In order to estimate the random error of the finally corrected fluxes, the propagation of error through the corrections has to be taken into account, especially for the estimation of long-term NEE (Liu et al., 2006). First, we multiplied the errors with the same spectral scaling factor as the fluxes to account for spectral attenuation. Then, we used Eq. (1) and (2) from Burba et al. (2008) to apply the WPL correction to the flux errors. Following basic concepts of error propagation, we corrected the random uncertainties the same way as if they were fluxes but adding them up in rooted quadrature using Eq. (7) for random error of water vapor flux and Eq. (8) for random error of CO_2 flux.

$$RE_E = (1+\mu\sigma)\sqrt{{RE_{E_0}}^2 + (\frac{RE_H}{\rho C_p}\frac{\rho_c}{T_a})^2} \tag{7}$$

$$RE_{F_C} = \sqrt{{RE_{F_{C0}}}^2 + (\mu\frac{RE_E}{\rho_d}\frac{\rho_c}{1+\mu\sigma})^2 + (\frac{RE_H}{\rho C_p}\frac{\rho_c}{T_a})^2} \tag{8}$$

RE_E and RE_{F_C} are the WPL-corrected water vapor and CO_2 flux errors (kg m^{-2} s^{-1}). RE_{E_0} and $RE_{F_{C0}}$ are the initial water vapor and CO_2 flux errors (kg m^{-2} s^{-1}), not corrected for WPL, but already multiplied by the spectral correction factors. RE_H is the sensible heat flux error, already corrected for WPL and spectral correction factor (W m^{-2}). μ is the ratio of molar masses of air to water ($\mu = 1.6077$), σ is the ratio of the mean water vapor density (ρ_v in kg m^{-2} s^{-1}) to mean dry air density (ρ_d in kg m^{-2} s^{-1}). ρ_c is the mean ambient CO_2 density (kg m^{-2} s^{-1}) and ρ is the mean total air mass density (kg m^{-2} s^{-1}). C_p is the air heat capacity (J kg^{-1} K^{-1}). The a posteriori sensor self heating correction (Sect. 2.6) does not include other scalars with quantified random error within its equations. Hence, the propagated random CO_2 flux error remains the same before and after self heating correction.

https://doi.org/10.5194/essd-2020-63
Preprint. Discussion started: 17 June 2020

3 Results

3.1 Drift correction

Figure 3 illustrates how the drift correction works quite well. Before drift correction, the CO_2 mixing ratios were underestimated substantially. Note the rapid divergence from the model after user calibrations were performed in 2009, 2012 and 2019. In June 2017 the original sensor was replaced with another one that was factory calibrated in March 2016. The drift correction eliminates the daily divergence from the modeled background concentration while keeping high frequency fluctuations for computation of the 30-min averaged fluxes. Remember that the drift correction applies an offset to the raw data and is subject to the subsequent flux calculation and correction procedures. Before application of WPL and spectral attenuation terms, the corrected fluxes yielded higher carbon uptake during daytime and summer, than the uncorrected fluxes. If the WPL and spectral attenuation correction is taken into account, the carbon uptake of the drift corrected fluxes gets considerably smaller than the uncorrected fluxes, especially during times with high sensible heat fluxes (see Fig. 7). The findings are in compliance with instrument theory of operation and the results from numerical simulations and field data analysis as conducted by Fratini et al. (2014) and with Serrano-Ortiz et al. (2008), who analyzed the propagation of a systematical underestimation of the CO_2 concentration on the CO_2 fluxes via the WPL terms.

3.2 Data availability and quality filtering

Table A1 lists the overall CO_2 and H_2O flux data availability after raw data processing, QC filtering and despiking, relative to the respective year. Figure 4 shows the data availability of the CO_2 fluxes throughout the individual years before and after gap filling (see also Sect. 2.7). The overall data availability differs substantially between the years. In 2013 more than 90 % of the data are missing. In 2014 the complete winter period is missing and about one year of data is missing from May 2018 to May 2019. Continuous data gaps of up to six months occur irregularly throughout the whole data set, whereas shorter gaps can be found within periods of continuously available data. The large gaps occurred mainly due to hardware errors and power shortages whereas smaller gaps are caused by raw data processing and subsequent filtering of fluxes with poor quality or due to violation of basic EC assumptions (see Sect. 2.2 and 2.4). Two periods with obviously corrupted flux measurements were excluded from the data set right after raw data processing. CO_2 and H_2O fluxes and concentrations were discarded from 2012-01-30 02:00 to 2012-08-31 15:00 and from 2018-06-01 00:00 to 2018-06-30 23:30 due to sensor malfunctioning. All times are in China Standard Time (CST, UTC+8). For the years 2007 to 2011, as well as for 2017, more than 50 % of the CO_2 fluxes are available. NEE gap filling increased the overall data availability for CO_2 fluxes from 48.3 % to 66.2 % in total, with seven complete years. The data set contains quality flags for each flux, indicating whether it was gap filled and how well the gap filling mechanism performed (Reichstein et al., 2005). The quality of the gap filled fluxes was derived by treating individual available values as data gaps and filling them as if they were real data gaps. When aggregating the residuals to an overall error estimate of the model performance, autocorrelation has to be taken into account because no independent training data is available. The model-data residuals were checked for empirical autocorrelation, indicated positive autocorrelation until a lag

https://doi.org/10.5194/essd-2020-63
Preprint. Discussion started: 17 June 2020

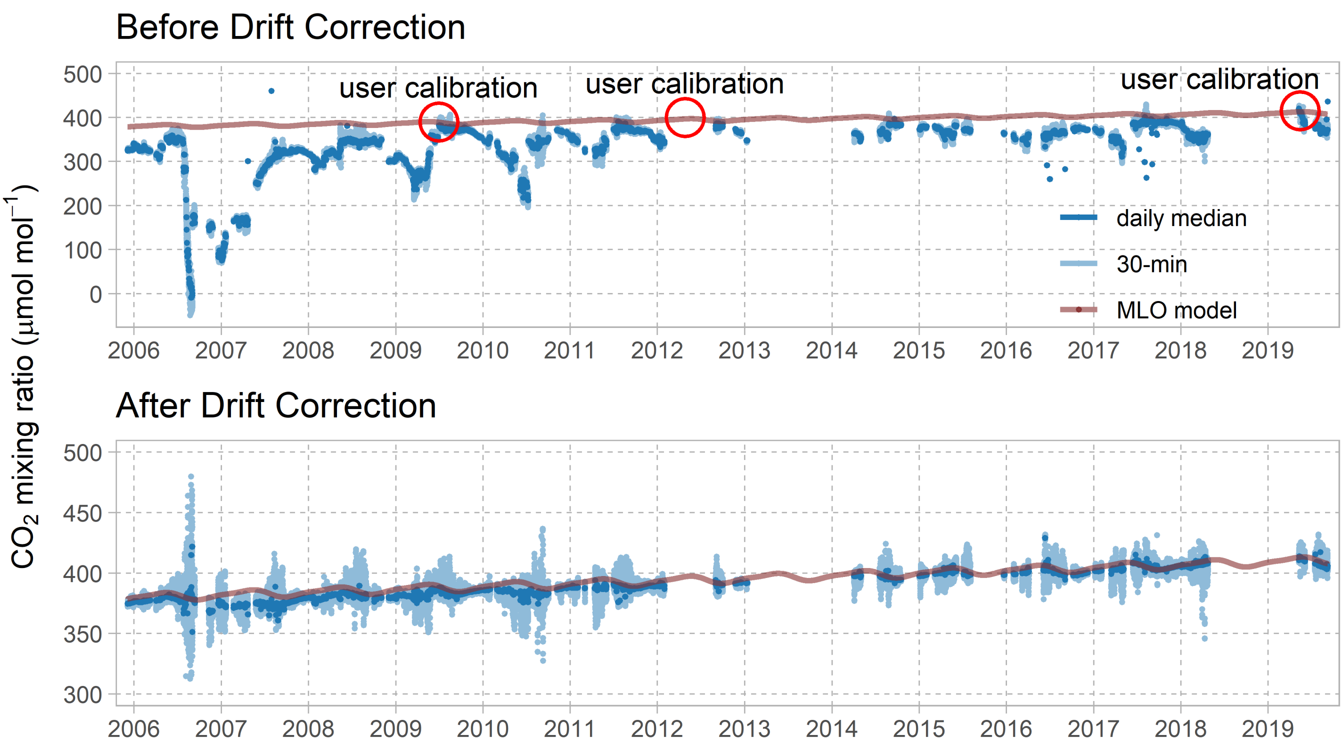

Figure 3. Daily median and 30-min CO_2 dry air mixing ratios and modeled CO_2 background concentration before and after drift correction. CO_2 mixing ratios have been checked for repeating values and outliers using the same algorithms as in Sect. 2.4. Please note the different y-axis scales.

of up to 65 records, decreasing the number of effective observations from 70758 to 8712. Taking this into account, Pearsons correlation coefficient is 0.83 with a root mean square error (RMSE) of 2.6 µmol m^{-2} s^{-1}.

3.3 Wind field analysis

Figure 2 shows how constructions changed in 2009, 2010, 2012 and 2019. It was not possible to assess when exactly the different buildings were constructed, hence we focused on the single most severe change, the set up of the two-storey main building in 2010. To assess the impact on the wind field, we calculated cumulative flux footprints (Fig.5) and wind rose plots for wind speed and TKE (Fig. 6) before and after 2010. It is to note that the wind regime is superimposed by large and small scale circulation systems. During summer, the Indian and East Asian summer monsoon blow from the southern directions and during winter, the westerlies provide air masses from western directions. Furthermore, the wind may be deflected along the Nyainqêntanglha range and exhibits a diurnal pattern due to a land – lake circulation system, caused by the large water masses of Nam Co (see also Biermann et al., 2014). Nevertheless, the differences before and after 2010 are clearly identifiable. A shift in the wind direction contribution away from the building and towards more western directions can be observed. Furthermore,

Open Access Earth System Science Data Discussions

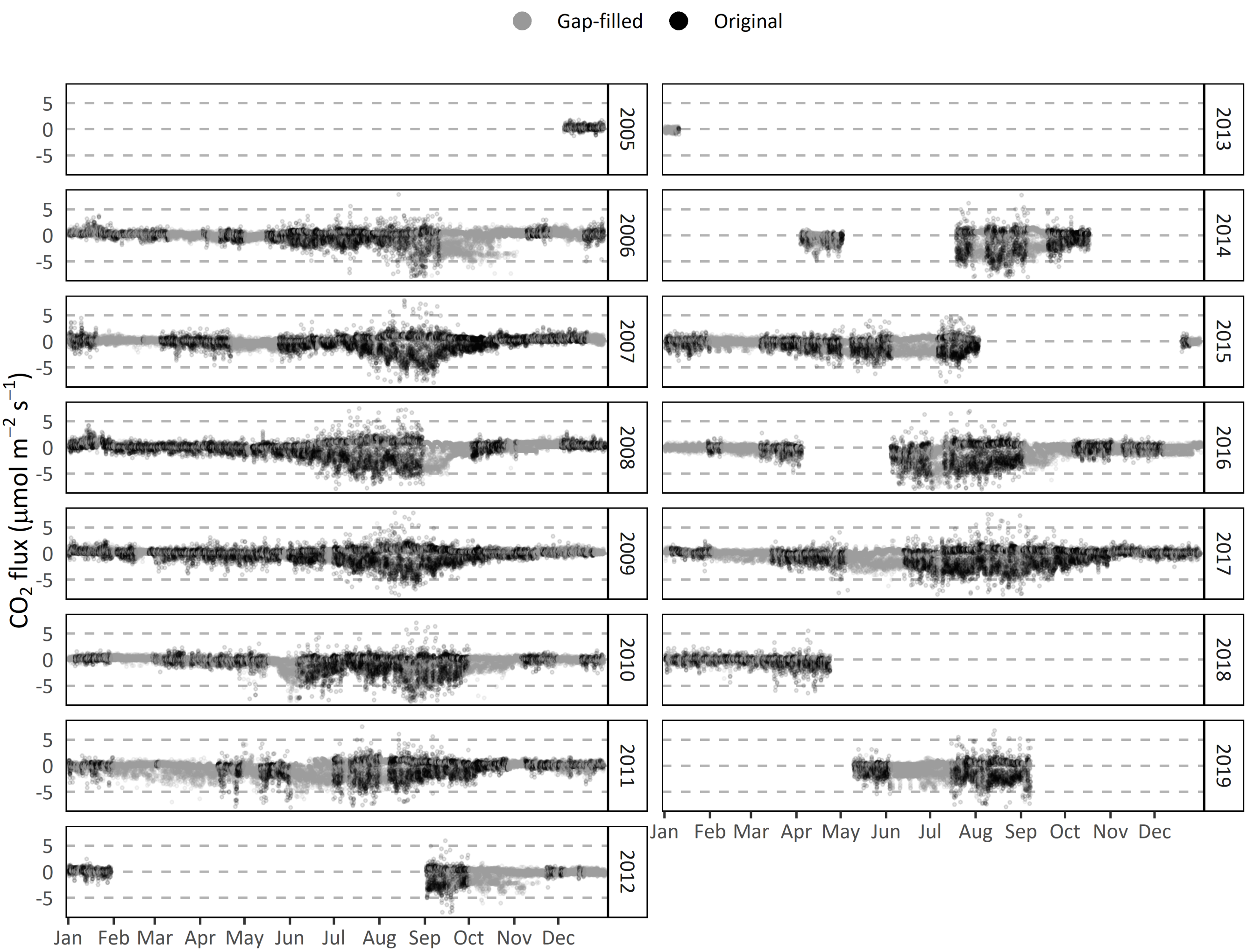

Figure 4. Data Availability after gap filling using REddyProc. Design modified from Holl et al. (2019).

wind speed and TKE increase substantially in western direction while decreasing in the direction of the main building. The cumulative footprints show complementary behavior. The main source area is a 150 m circular around the EC station, covering the buildings and sealed area, as well as the alpine steppe ecosystem within and outside the fenced area. In general, the size of the footprint gets smaller the stronger the atmosphere is mixed. The footprints at NAMORS follow this scheme, indicating an increase of the turbulent mixing in the lee of the different buildings. Fluxes ≥ 50 % contribution from the disturbed areas were excluded from further analyses. The ROI boundary is indicated in Fig. 2.

https://doi.org/10.5194/essd-2020-63
Preprint. Discussion started: 17 June 2020

Open Access Earth System Science Data Discussions

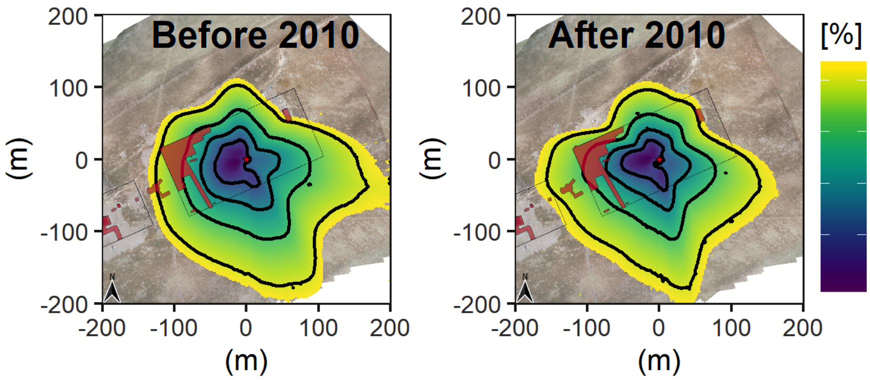

Figure 5. Cummulative flux footptints before and after the construction of the main building in 2010. The point $x = 0$ and $y = 0$ represents the position of the Eddy Covariance station. The disturbed (sealed) areas are illustrated by red polygons. Aerial images provided by Guoshuai Zhang.

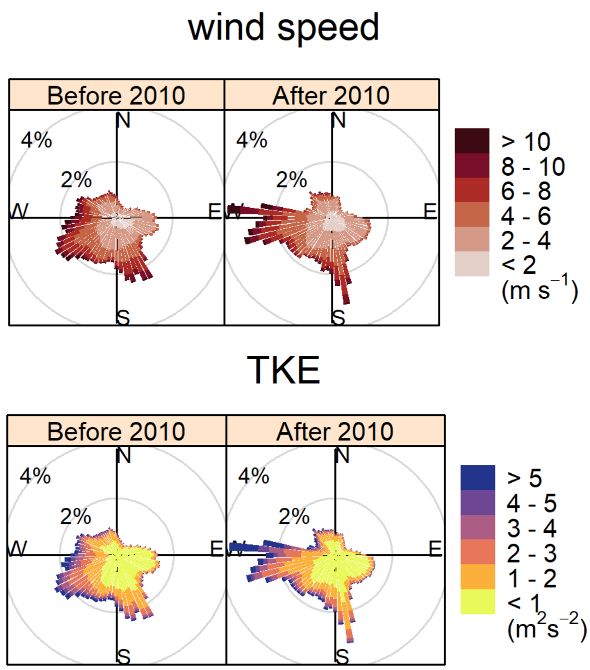

Figure 6. Wind roses showing the wind speed distribution and turbulent kinetic energy (TKE) in 5 ° binned wind directions at NAMORS EC station before and after 2010

https://doi.org/10.5194/essd-2020-63
Preprint. Discussion started: 17 June 2020

Table 2. The bounding conditions for the adjustment of the inclined sensor in Tibet

	Tbot_Ti	Ttop_Ti	Slope of Fc versus Air T, at Ta < -15 °C, (× 1000; the closer to zero the better)	Number of negative daily corrections at Ta < 0 °C (the smaller the better)
	0	100	0.38	1501
	20	80	0.09	675
	40	60	-0.21	133
	50	50	-0.36	49
	55	45	-0.43	12
	60	40	-0.50	2
Optimal weight for Tibet	**61**	**39**	**-0.52**	**1**
	62	38	-0.53	1
	63	37	-0.55	1
	64	36	-0.56	1
	65	35	-0.58	0
	70	30	-0.65	0
	80	20	-0.80	0
Vertical sensor in Nebraska	**100**	**0**	**-1.10**	**0**

3.4 Sensor self heating correction

The sensor self heating correction was applied during cold conditions (air temperature < 0 °C) after it was adjusted to meet local site conditions. Following Oechel et al. (2014), the weighting factors were iteratively chosen according to the flux-to-air temperature slope closest to zero below -15 °C while keeping the smallest number of mean daily negative corrections below 0 °C. Table 2 shows the bounding conditions for the weighting factors. With 61 % to 39 % weighting, the corrected daily CO_2 fluxes at temperatures below -15 °C had minimal slope with air temperature while allowing one negative daily correction at temperatures below 0 °C. Increasing the weighting factor led to steeper CO_2 flux-to-air temperature slope, which is physiologically unlikely. Decreasing the weighting factor led to a higher number of negative daily corrections which is implausible from the fundamental thermal exchange between the instrument which is controlled at +30 °C and ambient air temperatures below 0 °C. Figure 7 shows that the apparent CO_2 uptake during cold conditions was efficiently removed by the correction. The heating correction had the greatest effect during daytime when solar radiation additionally heats the inclined sensor. Before the correction, the fluxes were small but negative, suggesting CO_2 uptake even during very cold conditions. After the correction, the fluxes remained small but became positive, suggesting small respiration activity. Although the standard deviation of the mean daily corrections crossed the zero in almost all cases, the resulting fluxes are significantly different from zero ($p < 0.05$) while we allowed one occurrence of a negative daily heating correction.

https://doi.org/10.5194/essd-2020-63
Preprint. Discussion started: 17 June 2020

Open Access Earth System Science Data Discussions

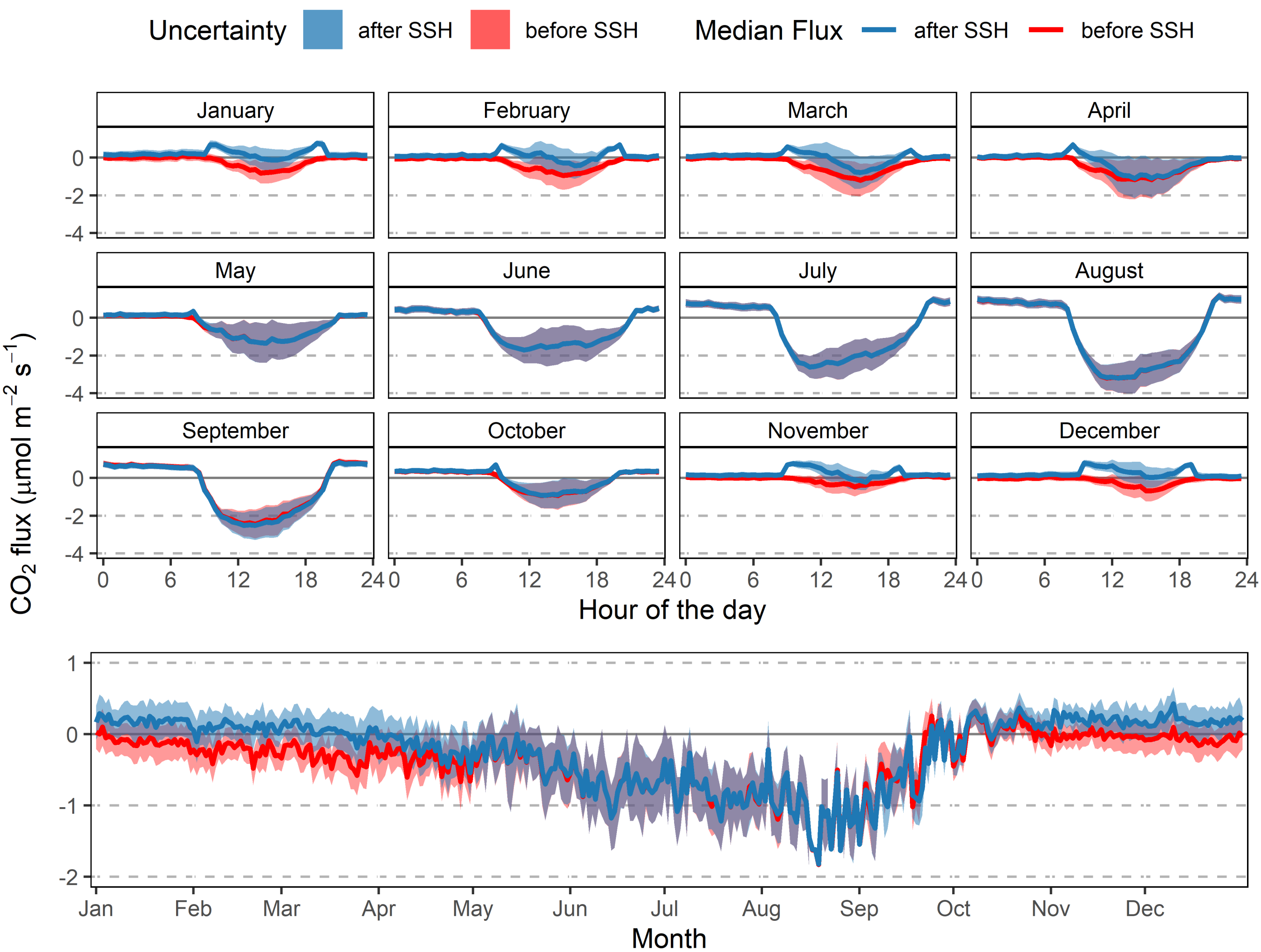

Figure 7. Monthly median daily course and annual course of daily median of the CO_2 flux and random uncertainty before and after sensor self heating correction (i.e. "SSH") of the years 2005 to 2019

4 Discussion

To produce an accurate and consistent time series of CO_2 fluxes, we applied several correction procedures and rigorously checked for data quality constraints during the long observation period, spanning almost 15 years. Nevertheless, some uncertainties remain, mainly due to technical and logistical constraints, as well as limited documentation of the measurements.

We applied the drift correction in order to remove a systematic bias in concentration measurements. Although the correction procedure itself works well, there are certainly other effects that could reduce the effective removal of the concentration drift. The use of the Mauna Loa time series as input for the model, which was used to derive the offset between measured and "real"

https://doi.org/10.5194/essd-2020-63
Preprint. Discussion started: 17 June 2020

CO_2 concentration, may be responsible for some degree of error. First, the measurements at Mauna Loa represent the northern hemisphere background CO_2 concentration, which does not necessarily mean, that they also represent the CO_2 concentrations at our study site. Second, the value used to estimate the offset was derived from a model. This approach somewhat smoothes the time series and generates the same annual pattern for every year while applying a constant rise in CO_2 concentrations. There is a good agreement between the two time series when sensor calibrations have just been conducted (red circles in 2009, 2012 and 2019 in Fig. 3). Concerning the drift correction of the H_2O measurements, the offset was derived from adjacent low frequency measurements of relative humidity, air temperature and air pressure. Although the approach itself is robust, there may be some degree of uncertainty due to the limited long term stability of the measurements which is claimed by the manufacturer with "better than 1 % RH per year" (Vaisala).

During the long observation period the surrounding of the EC system was subject to rather profound changes in constructions and scientific infrastructure. The wind regime changed substantially with the construction of the two-storey main building in 2010. The horizontal wind is forced to flow around this large obstacle, thereby increasing wind speeds and turbulent mixing reaching the EC system from western direction. Although the other constructions seem not to exhibit such a profound impact on the horizontal wind speed, some stronger turbulent mixing can be observed in the lee of the smaller buildings, such as the PBL container and the laboratory. The footprints display a complementary pattern, with smaller extend in areas with increased turbulent mixing. To address a possible influence by human activity, fluxes with large contributions (i.e. ≥ 50 %) beyond the ROI should be excluded from further analyses.

The use of a pre-2010 model of the Li-7500 open path IRGA requires the correction for apparent off-season CO_2 uptake due to air density fluctuations in the measurement path of the sensor (i.e. sensor self heating correction). We calibrated the procedure to meet local site conditions using the approach by Oechel et al. (2014) that relies on the identification of conditions with negligible CO_2 efflux. For the definition of these conditions, the same concerns as already mentioned by Oechel et al. (2014) also apply to our study: While, e.g. Wang et al. (2016) found carbon exchange of Tibetan alpine steppe during winter close to zero, it is still likely that even under the coldest conditions, microbial respiration may result in a temperature-dependent small source of CO_2 (Panikov et al., 2006). Hence, the actual CO_2 efflux may be larger than reported here due to an underestimation of the heating correction. Furthermore, the adjustment of the inclination presented above relies on significant empiricism and a number of assumptions, which add up to the already significant assumptions made by Burba et al. (2008) for the heating correction of a vertical aligned sensor. Hence, the method still represents a site-specific approximation which should be subject to optimization and automation approaches.

While systematic errors can be corrected efficiently, random errors may only be quantified in order to derive the overall precision of the measurements. Figure 7 shows the monthly median daily course of the CO_2 fluxes and their random uncertainties (Finkelstein and Sims, 2001) after correction for spectral attenuation and air density fluctuations (WPL and sensor self heating) from every available measurement throughout the long time series (without gap-filled values). When using an open path IRGA to determine gas densities, errors in the measurement of fluxes do not propagate proportionally through the WPL algorithm. In fact, the magnitude of these errors depends strongly on the sensible heat flux (Liu et al., 2006). Hence, the random flux errors are especially pronounced during daytime and summer, when sensible heat fluxes are large. During winter (November

https://doi.org/10.5194/essd-2020-63
Preprint. Discussion started: 17 June 2020

to February), the random error oftentimes exceeds the magnitude of the fluxes. The random uncertainty estimate described above represents a conservative value, as it specifically addresses the turbulence sampling error while neglecting other sources of random flux errors such as instrument noise and footprint variability.

One uncertainty, about the type of alpine steppe that the fluxes are supposed to represent, still exists. The whole NAMORS station was fenced in 2006, thus preventing the otherwise ubiquitous livestock from grazing in the footprint area. Wei et al. (2012) carried out chamber measurements within and outside the fenced area at the Nam Co station during the growing seasons of 2009 and 2010. The period of 4 years of livestock exclosure significantly increased above ground biomass which possibly led to lower soil temperatures due to shading effects. While the authors did not find a significant effect on CO_2 emission patterns during the two growing seasons, CO_2 emissions tended to be less sensitive to temperature change (i.e. lower Q_{10} value). Their findings are corroborated by Hafner et al. (2012) who used ^{13}C pulse labeling to assess the carbon cycle of a montane *Kobresia* pasture with moderate grazing and a 7-year-old grazing exclosure plot in the province of Qinghai on the north-eastern TP. While the total CO_2 efflux of the grazed and ungrazed grasslands remained similar, the grazing exclosure had a negative effect on organic carbon stocks in the upper 15 cm of the soil profile due to decreased total carbon input into the soil by plants and enhanced decomposition of medium and long term carbon stocks. The different processes governing the carbon cycle for grazed and ungrazed conditions have to be taken into account when drawing any conclusions on the ecosystem-atmosphere exchange from the site at Nam Co.

5 Related Work

Studies on carbon cycling on the central Tibetan Plateau have focused mainly on the *Kobresia* pastures (e.g, Ohtsuka et al., 2008; Babel et al., 2014; Zhang et al., 2016, 2018). The alpine *Kobresia* pastures represent an overall small sink of carbon dioxide, but its strength is highly variable within a year, as well as between several years (Gu et al., 2003; Kato et al., 2004, 2006; Saito et al., 2009). While alpine pastures have been studied extensively, the alpine steppe ecosystem has experienced relatively little interest, although it covers a much larger area. This can be explained by difficult accessibility and corresponding under-representation of (micro-) meteorological measurements. While the principal drivers of ecosystem-atmosphere CO_2 exchange seem to be similar in alpine steppe and pasture ecosystems, Ganjurjav et al. (2016) showed that warming significantly stimulated plant growth in the alpine pastures, but reduced growth and diversity in the alpine steppe ecosystem. Findings for the alpine steppe ecosystem suggest overall high correlation between soil water content and CO_2 fluxes, while it could not be clarified, whether the alpine steppe acts as an overall sink or source of CO_2 (Zhu et al., 2015; **?**). The fluxes varied substantially between the years depending on onset and strength of the monsoonal precipitation and temperature, indicating a close relationship to the strong seasonality on the TP. Interestingly, the high solar radiation seems to hamper diurnal carbon uptake by exceeding the maximum photosynthetic capacity during noon. Wei et al. (2012) conducted chamber measurements at Nam Co, corroborating the small sink strength for the growing seasons 2009 and 2010. This study is the first to report long-term, year-round CO_2 fluxes from the alpine steppe ecosystem which may be used to better understand carbon cycling under accelerated climate change scenarios.

https://doi.org/10.5194/essd-2020-63
Preprint. Discussion started: 17 June 2020

6 Conclusions

Here, we present the first long term eddy covariance (EC) CO_2 and H_2O flux measurements from the alpine steppe ecosystem which covers roughly 800,000 km^2 on the central Tibetan Plateau. The harsh environmental conditions and the remote location at > 4500 m above sea level make continuous and high-quality measurements especially challenging. To ensure meaningful flux estimates, we applied rigorous quality filtering rules and analyzed the turbulent flow regime to identify erroneous data. We efficiently removed a drift in mean concentration measurements, possibly caused by dirt contamination in the optical path and aging internal chemicals of the IRGA(Fratini et al., 2014). Furthermore, we corrected the CO_2 flux measurements for sensor self heating effects during cold conditions. Following Oechel et al. (2014), we were able to address the site-specific inclination of the open path IRGA rather than using the default corrections factors for vertically aligned sensors (Burba et al., 2008). The wind direction distributions of wind speed and TKE, as well as the analysis of cumulative footprints suggest that the several buildings which were constructed in close vicinity of the tower do exert some influence on the flow regime while not violating basic EC assumptions. Nevertheless, fluxes originating mainly from the disturbed areas should be excluded from further analyses as they may be compromised by human activities. Data availability of CO_2 fluxes after quality filtering and gap filling is quite different for individual years. While seven complete years of CO_2 ecosystem-atmosphere exchange are available, the filled data gaps are quite large, covering up to two months and should therefore be interpreted carefully. Unfortunately, the whole research station was fenced in 2006, thus preventing the otherwise ubiquitous yak, goat and sheep from grazing within the footprint. While biogeochemical cycles react quite slowly on the grazing exclosure, there is certainly some influence on vegetation and soil properties which should be subject to further examination. Nearly 15 years of consistently processed and quality controlled CO_2 flux data from the large but underrepresented Tibeten alpine steppe ecosystem are a valuable addition to further deepen the knowledge on carbon cycling in high alpine grassland ecosystems, which are especially vulnerable to global warming. The presented data set covers CO_2 and H_2O fluxes with quality flags for each processing step, footprint modeling and NEE gap filling results, as well as auxiliary measurements of meteorological variables and can be accessed via https://www.doi.org/10.5281/zenodo.3733203 (Nieberding et al., 2020b). This comprehensive data set allows potential users to put the gas flux dynamics into context with ecosystem properties, potential flux drivers and allows for comparison with other data sets.

7 Code and data availability

The data set was uploaded to Zenodo and is freely available under https://www.doi.org/10.5281/zenodo.3733203 (Nieberding et al., 2020b). Furthermore, the data set is available on the National Tibetan Plateau Center and can be accessed through https://www.doi.org/10.11888/Meteoro.tpdc.270333 (Nieberding et al., 2020a) after user registration on the website. The data sets are published under Creative Commons Attribution 4.0 International (CC BY 4.0) license. The R scripts used in this study are provided in the supplementary material of this manuscript.

https://doi.org/10.5194/essd-2020-63
Preprint. Discussion started: 17 June 2020

Appendix A: Processing of meteorological parameters

The PBL tower in close vicinity to the EC system provides additional measurements of air temperature (Ta), relative humidity (RH), wind speed (WS) and wind direction (WD) in several heights, as well as soil temperature (Ts), soil moisture (SMC) and soil heat flux (SHF) in several depths (see Sect. 2.1). A four component radiometer provides measurements of short and long wave incoming and outgoing radiation (SWin, LWin, SWout, LWout, respectively) and a net radiometer provides global radiation (GR). Furthermore, measurements of air pressure (Pa) are available. As a first step, time periods with obviously incorrect measurements were removed. Secondly, we set upper and lower thresholds for every measurement in order to removed physically implausible values from the time series: 30 °C < Ta < -35 °C; 100 % < RH / SMC < 0 %; 1000 W m^{-2} < SHF < -500 W m^{-2}; 1500 W m^{-2} < GR / SWin / SWout (values < 0 W m^{-2} were set to zero); 410 W m^{-2} < LWin < 75 W m^{-2}; 750 W m^{-2} < LWout < 150 W m^{-2}; 600 hPa < Pa < 500 hPa. The soil temperature in 20 cm depth was additionally despiked using the same method as in Sect. 2.4. In order to produce a time series as complete as possible, we merged biometeorological variables when possible. The low frequency air temperature and relative humidity measurements from the EC tower were filled step wise with the respective measurements from the different heights of the PBL tower, depending on their correlation (2 m > 4 m > 1.5 m > 10 m > 20 m). For Ts, the measurements from 0 cm depth were filled with the measurements from 10 cm and 20 cm depth. For SMC and SHF, the measurements from 10 cm depth were filled with the respective measurements from 20 cm depth. For the short and long wave radiation components, additional measurements for the years 2016 and 2017 were available and used when needed. As a last step, data gaps up to one hour (two time-steps) were linearly interpolated. The resulting time series were used as biometeorological input data for EddyPro and are supplied with the data set.

https://doi.org/10.5194/essd-2020-63
Preprint. Discussion started: 17 June 2020

Table A1. Data availability after individual processing steps. All units in % of the whole year, respectively

	CO_2 fluxes				H_2O fluxes		
Year	Raw	QC filtering	Fetch filtering	Gap filling	Raw	QC filtering	Fetch filtering
2005	7.3	5.8	3.9	7.4	7.3	5.4	3.7
2006	63.5	48.2	33.1	100	63.6	46.9	32.9
2007	75.6	59.3	49.1	100	75.5	60.1	50.0
2008	86.9	68.0	53.7	100	84.3	65.2	51.6
2009	92.8	74.5	52.8	100	92.6	72.3	52.1
2010	71.4	55.6	37.2	100	71.4	54.1	37.2
2011	65.0	50.4	35.3	100	65.0	49.7	35.5
2012	19.2	15.1	10.3	41.3	19.2	14.9	10.1
2013	0.2	0.2	0.1	2.7	0.2	0.2	0.1
2014	26.5	21.1	16.6	32.8	26.2	20.4	16.3
2015	39.6	31.0	22.7	62.0	39.6	30.1	22.3
2016	48.2	38.7	27.6	83.4	48.2	37.9	27.3
2017	77.0	60.0	45.0	100	76.9	58.6	44.3
2018	30.5	23.4	13.6	30.9	30.5	21.6	12.8
2019	21.4	15.9	13.7	33.1	22	15.9	13.6

Author contributions. TS, CW and YM conceptualized and administered the research activity planning and execution and acquired funds for it. FN, MOA and YW conducted the investigation. FN, CW, GF and MOA analyzed the data. FN and MOA created the visualizations. FN wrote the original draft. FN, CW, GF, MOA, YW, YM and TS reviewed and edited the original draft.

Competing interests. The authors declare that they have no conflict of interest.

Acknowledgements. We thank George Burba for providing the Excel spreadsheets from which the calculations of the sensor self heating correction were derived. Special thanks go to Guoshuai Zhang and Binbin Wang who were a great help during field work and to Guoshuai Zhang for providing the aerial images used in Figs. 1, 2 and 5. We thank Prof. Li Jia from the Institute of Remote Sensing and Digital Earth (CAS) for providing additional radiation data. This research is a contribution to the International Research Training Group "Geo-ecosystems in transition on the Tibetan Plateau (TransTiP)", funded by Deutsche Forschungsgemeinschaft (DFG grant 317513741 / GRK 2309). It was supported by the Second Tibetan Plateau Scientific Expedition and Research (STEP) program (2019QZKK0103), the Strategic Priority Research Program of Chinese Academy of Sciences (XDA20060101) and the National Natural Science Foundation of China (91837208). We acknowledge support by the Open Access Publication Funds of the Technische Universität Braunschweig.

References

Aubinet, M., Vesala, T., and Papale, D.: Eddy Covariance, Springer Netherlands, Dordrecht, 2012.

Babel, W., Biermann, T., Coners, H., Falge, E., Seeber, E., Ingrisch, J., Schleuß, P.-M., Gerken, T., Leonbacher, J., Leipold, T., Willinghöfer, S., Schützenmeister, K., Shibistova, O., Becker, L., Hafner, S., Spielvogel, S., Li, X., Xu, X., Sun, Y., Zhang, L., Yang, Y., Ma, Y., Wesche, K., Graf, H., Leuschner, C., Guggenberger, G., Kuzyakov, Y., Miehe, G., and Foken, T.: Pasture degradation modifies the water and carbon cycles of the Tibetan highlands, Biogeosciences, 11, 6633–6656, https://doi.org/10.5194/bg-11-6633-2014, 2014.

Biermann, T., Babel, W., Ma, W., Chen, X., Thiem, E., Ma, Y., and Foken, T.: Turbulent flux observations and modelling over a shallow lake and a wet grassland in the Nam Co basin, Tibetan Plateau, Theoretical and Applied Climatology, 116, 301–316, https://doi.org/10.1007/s00704-013-0953-6, 2014.

Burba, G. G., McDermitt, D. K., Grelle, A., Anderson, D., and XU, L.: Addressing the influence of instrument surface heat exchange on the measurements of CO 2 flux from open-path gas analyzers, Global Change Biology, 14, 1854–1876, https://doi.org/10.1111/j.1365-2486.2008.01606.x, 2008.

Cuo, L. and Zhang, Y.: Spatial patterns of wet season precipitation vertical gradients on the Tibetan Plateau and the surroundings, Scientific reports, 7, 5057, https://doi.org/10.1038/s41598-017-05345-6, https://doi.org/10.1038/s41598-017-05345-6, 2017.

Falge, E., Baldocchi, D., Olson, R., Anthoni, P., Aubinet, M., Bernhofer, C., Burba, G., Ceulemans, R., Clement, R., Dolman, H., Granier, A., Gross, P., Grünwald, T., Hollinger, D., Jensen, N.-O., Katul, G. G., Keronen, P., Kowalski, A., Lai, C. T., Law, B. E., Meyers, T., Moncrieff, J., Moors, E., Munger, W., Pilegaard, K., Rannik, Ü., Rebmann, C., Suyker, A., Tenhunen, J., Tu, K., Verma, S., Vesala, T., Wilson, K., and Wofsy, S.: Gap filling strategies for defensible annual sums of net ecosystem exchange, Agricultural and Forest Meteorology, 107, 43–69, https://doi.org/10.1016/S0168-1923(00)00225-2, 2001.

Finkelstein, P. L. and Sims, P. F.: Sampling error in eddy correlation flux measurements, Journal of Geophysical Research: Atmospheres, 106, 3503–3509, https://doi.org/10.1029/2000JD900731, 2001.

Foken, T. and Wichura, B.: Tools for quality assessment of surface-based flux measurements, Agricultural and Forest Meteorology, 78, 83–105, https://doi.org/10.1016/0168-1923(95)02248-1, 1996.

Foken, T., Göckede, M., Mauder, M., Mahrt, L., Amiro, B., and Munger, W.: Post-Field Data Quality Control, in: Handbook of micrometeorology, edited by Lee, X., Massman, W. J., and Law, B. E., vol. 29 of *Atmospheric and Oceanographic Sciences Library*, pp. 181–208, Kluwer Academic Publishers, Dordrecht and Boston and London, 2004.

Fratini, G., McDermitt, D. K., and Papale, D.: Eddy-covariance flux errors due to biases in gas concentration measurements: origins, quantification and correction, Biogeosciences, 11, 1037–1051, https://doi.org/10.5194/bg-11-1037-2014, 2014.

Ganjurjav, H., Gao, Q., Gornish, E. S., Schwartz, M. W., Liang, Y., Cao, X., Zhang, W., Zhang, Y., Li, W., Wan, Y., Li, Y., Danjiu, L., Guo, H., and Lin, E.: Differential response of alpine steppe and alpine meadow to climate warming in the central Qinghai–Tibetan Plateau, Agricultural and Forest Meteorology, 223, 233–240, https://doi.org/10.1016/j.agrformet.2016.03.017, 2016.

Gu, S., Tang, Y., Du, M., Kato, T., Li, Y., Cui, X., and Zhao, X.: Short-term variation of CO2 flux in relation to environmental controls in an alpine meadow on the Qinghai-Tibetan Plateau, Journal of Geophysical Research: Atmospheres, 108, 711, https://doi.org/10.1029/2003JD003584, 2003.

Hafner, S., Unteregelsbacher, S., Seeber, E., Lena, B., Xu, X., Li, X., Guggenberger, G., Miehe, G., and Kuzyakov, Y.: Effect of grazing on carbon stocks and assimilate partitioning in a Tibetan montane pasture revealed by 13CO2 pulse labeling, Global Change Biology, 18, 528–538, https://doi.org/10.1111/j.1365-2486.2011.02557.x, 2012.

https://doi.org/10.5194/essd-2020-63
Preprint. Discussion started: 17 June 2020

Holl, D., Wille, C., Sachs, T., Schreiber, P., Runkle, B. R. K., Beckebanze, L., Langer, M., Boike, J., Pfeiffer, E.-M., Fedorova, I., Bolshianov, D. Y., Grigoriev, M. N., and Kutzbach, L.: A long-term (2002 to 2017) record of closed-path and open-path eddy covariance CO₂ net ecosystem exchange fluxes from the Siberian Arctic, Earth System Science Data, 11, 221–240, https://doi.org/10.5194/essd-11-221-2019, 2019.

Kato, T., Tang, Y., Song, G., Hirota, M., Cui, X., Du, M., Li, Y., Zhao, X., and Oikawa, T.: Seasonal patterns of gross primary production and ecosystem respiration in an alpine meadow ecosystem on the Qinghai-Tibetan Plateau, Journal of Geophysical Research, 109, 711, https://doi.org/10.1029/2003JD003951, 2004.

Kato, T., Tang, Y., Gu, S., Hirota, M., Du, M., Li, Y., and Zhao, X.: Temperature and biomass influences on interannual changes in CO2 exchange in an alpine meadow on the Qinghai-Tibetan Plateau, Global Change Biology, 12, 1285–1298, https://doi.org/10.1111/j.1365-2486.2006.01153.x, 2006.

Kormann, R. and Meixner, F. X.: An Analytical Footprint Model For Non-Neutral Stratification, Boundary-Layer Meteorology, 99, 207–224, https://doi.org/10.1023/A:1018991015119, 2001.

Li, J., Yan, D., Pendall, E., Pei, J., Noh, N. J., He, J.-S., Li, B., Nie, M., and Fang, C.: Depth dependence of soil carbon temperature sensitivity across Tibetan permafrost regions, Soil Biology and Biochemistry, 126, 82–90, 2018.

Liu, H., Randerson, J. T., Lindfors, J., Massman, W. J., and Foken, T.: Consequences of Incomplete Surface Energy Balance Closure for CO2 Fluxes from Open-Path CO2/H2O Infrared Gas Analysers, Boundary-Layer Meteorology, 120, 65–85, https://doi.org/10.1007/s10546-005-9047-z, https://doi.org/10.1007/s10546-005-9047-z, 2006.

Ma, Y., Wang, Y., Wu, R., Hu, Z., Yang, K., Li, M., Ma, W., Zhong, L., Sun, F., Chen, X., Zhu, Z., Wang, S., and Ishikawa, H.: Recent advances on the study of atmosphere-land interaction observations on the Tibetan Plateau, Hydrology and Earth System Sciences, 13, 1103–1111, https://doi.org/10.5194/hess-13-1103-2009, 2009.

Mauder, M. and Foken, T.: Impact of post-field data processing on eddy covariance flux estimates and energy balance closure, Meteorologische Zeitschrift, 15, 597–609, https://doi.org/10.1127/0941-2948/2006/0167, 2006.

Mauder, M., Cuntz, M., Drüe, C., Graf, A., Rebmann, C., Schmid, H. P., Schmidt, M., and Steinbrecher, R.: A strategy for quality and uncertainty assessment of long-term eddy-covariance measurements, Agricultural and Forest Meteorology, 169, 122–135, https://doi.org/10.1016/j.agrformet.2012.09.006, 2013.

Miehe, G., Bach, K., Miehe, S., Kluge, J., Yongping, Y., La Duo, Co, S., and Wesche, K.: Alpine steppe plant communities of the Tibetan highlands, Applied Vegetation Science, 14, 547–560, https://doi.org/10.1111/j.1654-109X.2011.01147.x, 2011.

Miehe, G., Schleuss, P.-M., Seeber, E., Babel, W., Biermann, T., Braendle, M., Chen, F., Coners, H., Foken, T., Gerken, T., Graf, H.-F., Guggenberger, G., Hafner, S., Holzapfel, M., Ingrisch, J., Kuzyakov, Y., Lai, Z., Lehnert, L., Leuschner, C., Li, X., Liu, J., Liu, S., Ma, Y., Miehe, S., Mosbrugger, V., Noltie, H. J., Schmidt, J., Spielvogel, S., Unteregelsbacher, S., Wang, Y., Willinghöfer, S., Xu, X., Yang, Y., Zhang, S., Opgenoorth, L., and Wesche, K.: The Kobresia pygmaea ecosystem of the Tibetan highlands - Origin, functioning and degradation of the world's largest pastoral alpine ecosystem: Kobresia pastures of Tibet, The Science of the total environment, 648, 754–771, https://doi.org/10.1016/j.scitotenv.2018.08.164, 2019.

Moncrieff, J., Clement, R., Finnigan, J., and Meyers, T.: Averaging, Detrending, and Filtering of Eddy Covariance Time Series, in: Handbook of Micrometeorology: A Guide for Surface Flux Measurement and Analysis, edited by Lee, X., Massman, W., and Law, B., pp. 7–31, Springer Netherlands, Dordrecht, https://doi.org/10.1007/1-4020-2265-4_2, 2005.

https://doi.org/10.5194/essd-2020-63
Preprint. Discussion started: 17 June 2020

Moncrieff, J. B., Massheder, J. M., de Bruin, H., Elbers, J., Friborg, T., Heusinkveld, B., Kabat, P., Scott, S., Soegaard, H., and Verhoef, A.: A system to measure surface fluxes of momentum, sensible heat, water vapour and carbon dioxide, Journal of Hydrology, 188-189, 589–611, https://doi.org/10.1016/S0022-1694(96)03194-0, 1997.

NASA/METI/AIST/Japan Spacesystems, and U.S./Japan ASTER Science Team: ASTER Global Digital Elevation Model V003, distributed by NASA EOSDIS Land Processes DAAC, https://doi.org/10.5067/ASTER/ASTGTM.003, 2019.

Nieberding, F., Ma, Y., Wille, C., Fratini, G., Asmussen, M. O., Wang, Y., Ma, W., and Sachs, T.: A long term hourly eddy covariance dataset of consistently processed CO2 and H2O Fluxes from the Tibetan Alpine Steppe at Nam Co (2005 - 2019), National Tibetan Plateau Data Center, https://doi.org/10.11888/Meteoro.tpdc.270333, 2020a.

Nieberding, F., Ma, Y., Wille, C., Fratini, G., Asmussen, M. O., Wang, Y., Ma, W., and Sachs, T.: A long term hourly eddy covariance dataset of consistently processed CO2 and H2O Fluxes from the Tibetan Alpine Steppe at Nam Co (2005 - 2019) [Data set]., Zenodo, https://doi.org/10.5281/ZENODO.3733203, 2020b.

NOAA ESRL Global Monitoring Division: Atmospheric Carbon Dioxide Dry Air Mole Fractions from quasi-continuous measurements at Mauna Loa, Hawaii, Barrow, Alaska, American Samoa and South Pole. Compiled by K.W. Thoning, D.R. Kitzis, and A. Crotwell., https://doi.org/10.15138/yaf1-bk21.

Nölling, J.: Satellitenbildgestützte Vegetationskartierung von Hochweidegebieten des Tibetischen Plateaus auf Grundlage von plotbasierten Vegetationsaufnahmen mit multivariater statistischer Analyse: Ein Beitrag zum Umweltmonitoring, Diplomarbeit, Universität Marburg, Marburg, 2006.

Oechel, W. C., Laskowski, C. A., Burba, G., Gioli, B., and Kalhori, A. A. M.: Annual patterns and budget of CO 2 flux in an Arctic tussock tundra ecosystem, Journal of Geophysical Research: Biogeosciences, 119, 323–339, https://doi.org/10.1002/2013JG002431, 2014.

Ohtsuka, T., Hirota, M., Zhang, X., Shimono, A., Senga, Y., Du, M., Yonemura, S., Kawashima, S., and Tang, Y.: Soil organic carbon pools in alpine to nival zones along an altitudinal gradient (4400–5300m) on the Tibetan Plateau, Polar Science, 2, 277–285, https://doi.org/10.1016/j.polar.2008.08.003, 2008.

Panikov, N. S., Flanagan, P. W., Oechel, W. C., Mastepanov, M. A., and Christensen, T. R.: Microbial activity in soils frozen to below −39°C, Soil Biology and Biochemistry, 38, 785–794, https://doi.org/10.1016/j.soilbio.2005.07.004, 2006.

Papale, D., Reichstein, M., Aubinet, M., Canfora, E., Bernhofer, C., Kutsch, W., Longdoz, B., Rambal, S., Valentini, R., Vesala, T., and Yakir, D.: Towards a standardized processing of Net Ecosystem Exchange measured with eddy covariance technique: algorithms and uncertainty estimation, Biogeosciences, 3, 571–583, https://doi.org/10.5194/bg-3-571-2006, 2006.

Qiu, J.: China: The third pole, Nature, 454, 393–396, https://doi.org/10.1038/454393a, 2008.

Reichstein, M., Falge, E., Baldocchi, D., Papale, D., Aubinet, M., Berbigier, P., Bernhofer, C., Buchmann, N., Gilmanov, T., Granier, A., Grunwald, T., Havrankova, K., Ilvesniemi, H., Janous, D., Knohl, A., Laurila, T., Lohila, A., Loustau, D., Matteucci, G., Meyers, T., miglietta, F., ourcival, J.-m., Pumpanen, J., Rambal, S., Rotenberg, E., Sanz, M., Tenhunen, J., Seufert, G., Vaccari, F., Vesala, T., Yakir, D., and valentini, R.: On the separation of net ecosystem exchange into assimilation and ecosystem respiration: review and improved algorithm, Global Change Biology, 11, 1424–1439, https://doi.org/10.1111/j.1365-2486.2005.001002.x, 2005.

Richardson, A. D., Aubinet, M., Barr, A. G., Hollinger, D. Y., Ibrom, A., Lasslop, G., and Reichstein, M.: Uncertainty Quantification, in: Eddy Covariance: A Practical Guide to Measurement and Data Analysis, edited by Aubinet, M., Vesala, T., and Papale, D., pp. 173–209, Springer Netherlands, Dordrecht, https://doi.org/10.1007/978-94-007-2351-1_7, https://doi.org/10.1007/978-94-007-2351-1_7, 2012.

Saito, M., Kato, T., and Tang, Y.: Temperature controls ecosystem CO 2 exchange of an alpine meadow on the northeastern Tibetan Plateau, Global Change Biology, 15, 221–228, https://doi.org/10.1111/j.1365-2486.2008.01713.x, 2009.

https://doi.org/10.5194/essd-2020-63
Preprint. Discussion started: 17 June 2020

Serrano-Ortiz, P., Kowalski, A. S., Domingo, F., Ruiz, B., and Alados-Arboledas, L.: Consequences of Uncertainties in CO2 Density for Estimating Net Ecosystem CO2 Exchange by Open-path Eddy Covariance, Boundary-Layer Meteorology, 126, 209–218, https://doi.org/10.1007/s10546-007-9234-1, 2008.

Vaisala: Vaisala HUMICAP® Humidity and Temperature Probes HMP45A/D: HMP45A and HMP45D Operating Manual, https://www.vaisala.com/sites/default/files/documents/HMP45AD-User-Guide-U274EN.pdf.

Vickers, D. and Mahrt, L.: Quality Control and Flux Sampling Problems for Tower and Aircraft Data, Journal of Atmospheric and Oceanic Technology, 14, 512–526, https://doi.org/10.1175/1520-0426(1997)014<0512:QCAFSP>2.0.CO;2, 1997.

Wang, L., Liu, H., Shao, Y., Liu, Y., and Sun, J.: Water and CO2 fluxes over semiarid alpine steppe and humid alpine meadow ecosystems on the Tibetan Plateau, Theoretical and Applied Climatology, 131, 547–556, https://doi.org/10.1007/s00704-016-1997-1, 2016.

Wang, X., Pang, G., and Yang, M.: Precipitation over the Tibetan Plateau during recent decades: a review based on observations and simulations, International Journal of Climatology, 38, 1116–1131, https://doi.org/10.1002/joc.5246, 2018.

Webb, E. K., Pearman, G. I., and Leuning, R.: Correction of flux measurements for density effects due to heat and water vapour transfer, Quarterly Journal of the Royal Meteorological Society, 106, 85–100, 1980.

Wei, D., Ri, X., Wang, Y., Wang, Y., Liu, Y., and Yao, T.: Responses of CO2, CH4 and N2O fluxes to livestock exclosure in an alpine steppe on the Tibetan Plateau, China, Plant and Soil, 359, 45–55, https://doi.org/10.1007/s11104-011-1105-3, 2012.

Wutzler, T., Lucas-Moffat, A., Migliavacca, M., Knauer, J., Sickel, K., Šigut, L., Menzer, O., and Reichstein, M.: Basic and extensible post-processing of eddy covariance flux data with REddyProc, Biogeosciences, 15, 5015–5030, https://doi.org/10.5194/bg-15-5015-2018, 2018.

Yang, K., Wu, H., Qin, J., Lin, C., Tang, W., and Chen, Y.: Recent climate changes over the Tibetan Plateau and their impacts on energy and water cycle: A review, Global and Planetary Change, 112, 79–91, https://doi.org/10.1016/j.gloplacha.2013.12.001, 2014.

Yao, T., Xue, Y., Chen, D., Chen, F., Thompson, L., Cui, P., Koike, T., Lau, W. K.-M., Lettenmaier, D., Mosbrugger, V., Zhang, R., Xu, B., Dozier, J., Gillespie, T., Gu, Y., Kang, S., Piao, S., Sugimoto, S., Ueno, K., Wang, L., Wang, W., Zhang, F., Sheng, Y., Guo, W., Ailikun, Yang, X., Ma, Y., Shen, S. S. P., Su, Z., Chen, F., Liang, S., Liu, Y., Singh, V. P., Yang, K., Yang, D., Zhao, X., Qian, Y., Zhang, Y., and Li, Q.: Recent Third Pole's Rapid Warming Accompanies Cryospheric Melt and Water Cycle Intensification and Interactions between Monsoon and Environment: Multidisciplinary Approach with Observations, Modeling, and Analysis, Bulletin of the American Meteorological Society, 100, 423–444, https://doi.org/10.1175/BAMS-D-17-0057.1, 2019.

Zhang, T., Zhang, Y., Xu, M., Xi, Y., Zhu, J., Zhang, X., Wang, Y., Li, Y., Shi, P., Yu, G., and Sun, X.: Ecosystem response more than climate variability drives the inter-annual variability of carbon fluxes in three Chinese grasslands, Agricultural and Forest Meteorology, 225, 48–56, https://doi.org/10.1016/j.agrformet.2016.05.004, 2016.

Zhang, T., Zhang, Y., Xu, M., Zhu, J., Chen, N., Jiang, Y., Huang, K., Zu, J., Liu, Y., and Yu, G.: Water availability is more important than temperature in driving the carbon fluxes of an alpine meadow on the Tibetan Plateau, Agricultural and Forest Meteorology, 256-257, 22–31, https://doi.org/10.1016/j.agrformet.2018.02.027, 2018.

Zhou, Y., Webster, R., Viscarra Rossel, R. A., Shi, Z., and Chen, S.: Baseline map of soil organic carbon in Tibet and its uncertainty in the 1980s, Geoderma, 334, 124–133, https://doi.org/10.1016/j.geoderma.2018.07.037, 2019.

Zhu, Z., Ma, Y., Li, M., Hu, Z., Xu, C., Zhang, L., Han, C., Wang, Y., and Ichiro, T.: Carbon dioxide exchange between an alpine steppe ecosystem and the atmosphere on the Nam Co area of the Tibetan Plateau, Agricultural and Forest Meteorology, 203, 169–179, https://doi.org/10.1016/j.agrformet.2014.12.013, 2015.